10

Innovations in Antenna Systems for Communications

Chapter Editors: B. K. Lau, Z. Miers, A. Tatomirescu, S. Caporal Del Barrio, P. Bahramzy, P. Gentner, H. Li and G. Lasser

10.1 Introduction

As wireless communications continue to grow in importance by providing exciting new services beyond the conventional voice and text-only communications, antenna systems must evolve in order to keep up with ever increasing requirements and technical challenges. One prominent example is the demand for high data rates in mobile communications, due to data intensive applications such as interactive gaming and video streaming. Apart from the challenge of implementing multiple antennas in physically small terminals to support multiple-input multiple-output (MIMO)-enabled data rate enhancement, suitable measures are also needed to ensure that the antenna performance does not degrade due to proximity of the user and variability in the channel conditions. Moreover, the rapid adoption of machine-to-machine (M2M) communications and internet-of-things (IoT) concept also provides ample opportunities for innovations in antenna systems, including the use of smart antennas in RFID technology to enable smart wireless sensor nodes for tyre pressure monitoring.

In this context, Chapter 10 deals with recent advances and innovations in antenna systems for communications. Section 10.2 first examines the design of multiple antenna systems, focusing on the optimisation of antenna performance using decoupling techniques. Apart from designing MIMO terminal antennas, where moderate isolation (e.g., 10–15 dB) is sufficient, the section also presents new results on antenna decoupling for applications that require very high transmit-to-receive isolation (e.g., 80 dB for full duplex operation). As a promising new approach to provide efficient MIMO antennas, the growing field of antenna design using the theory of characteristic modes (TCMs) is summarised. Then, Section 10.3 explores the topic of smart reconfigurable

antennas, where antennas are designed to be frequency reconfigurable to fulfill extreme bandwidth requirements of long-term evolution (LTE) systems. The emphasis is on its application to architectures advocating very high transmit-to-receive isolation, since such architectures favour the use of antennas with narrow instantaneous bandwidth. More ambitious reconfigurable antenna structures that can be harmonised to the immediate environment including user and propagation channel are also introduced. In Section 10.4, the attention is turned towards RFID and sensor antenna innovations, with different antenna design and modelling issues discussed for a variety of applications, with operations in high frequency (HF), ultra high frequency (UHF), and ultra-wideband (UWB) bands.

Following the recent innovations in antenna design for various applications, Section 10.5 deals with the holistic characterisation and measurement of antenna performance. Topics covered include latest advances in performance metrics, modelling of the user-channel effects and antenna evaluation in realistic scenarios. One important message to convey in this section is that, ultimately, smart innovations in antenna systems are not meaningful if they cannot be proven to provide real performance benefits in real life operations. Lastly, Section 10.6 is dedicated to a discussion of antenna measurement techniques, especially on the measurement of antenna patterns. Although measurement of antenna parameters is not a new topic, many challenges remain in obtaining good quality measurements, including the effect of feed cable on small antenna measurement, accurate pattern measurement of millimeter wave (mmW) frequencies and distortion of antenna pattern measurement due to support structures.

10.2 MIMO Antenna Innovations

High transmission rates of next generation communication systems require significant attention to individual antenna element design. Implementing multiple antennas in both the base stations and user terminals is key to increasing the channel capacity without sacrificing additional frequency spectrum and transmit power. In theory designing both base station antennas as well as mobile terminals is well researched and documented. However, practical design constraints prevent traditional antenna implementations from performing well in MIMO systems. The compactness of today's terminals is one such constraint that complicates the design of MIMO antennas.

In an effort to solve some of the problems associated with implementing multiple antennas in mobile terminals, several areas of terminal antenna design are actively being researched. The most challenging application of MIMO for

mobile devices is given by the electrically small nature of mobile phones in the lower end of the frequency spectrum used in LTE. Different decoupling and decorrelating methods are discussed and evaluated further, ranging from the more straightforward antenna placement optimisation to some more complex methods such as the self-interference cancellation. Key design and implementation challenges are discussed with the focus on MIMO performance of the antenna system. Another approach to solving problems caused by compact MIMO terminals is through the use of TCMs. Characteristic modes allow a designer to determine all the orthogonal modes a structure is able to produce and determine where and how to feed these modes. This allows for optimal MIMO antenna placement as well as physical insights into how to feed each orthogonal mode [LLH11].

10.2.1 MIMO Antenna Decoupling and Optimisation

From a system perspective, the design of MIMO antennas on an electrically small ground plane is a complex optimisation problem due to the fact that the system's capacity depends on power balance, level, and correlation in each of the communication links which are a function of antenna pattern and channel properties [DFPS09]. The placement of the separate antenna elements has been investigated using multiple monopoles and inverted-F antenna (IFA) antennas on a card type ground plane [OC04, ANW11] for the higher frequencies used in LTE. A more general and systematic approach is presented in Karimkashi et al. [KKK11] where infinitesimal small dipoles are used to model the interactions between the antenna elements and the ground plane offering a fast optimisation process to enhance MIMO performance. However, the lower frequency bands of LTE are still not not addressed. Since the shape of gain pattern for electrically small antennas (ESAs) is very similar to a dipole pattern, a simplified metric using the efficiency and antenna correlation is presented for evaluating MIMO performance in Derneryd et al. [DSSW11]. This metric, also know as the multiplexing efficiency [TLY11], provides an efficient cost function for the multi-objective optimisation presented in Derneryd et al. [DSSW11] of the design for a dual band dual-antenna system which supports the 750–800 MHz and 2.5–2.7 GHz frequency bands.

Depending on the electrical size of the device, in some cases the optimal placement for the antenna elements of a MIMO antenna does not guarantee acceptable MIMO performance due to the high coupling between antennas. Thus, methods to cancel the coupling have been investigated in the past. These can be split into two main families, one containing methods to isolate the output ports of the antennas and the other focusing on decoupling the antennas.

Implementations from the first family can be seen as early as 1976 in Andersen and Rasmussen [AR76] followed by different embodiments of this concept as parasitic scatterers [LA12], a neutralisation line [CLD$^+$08], using a feeding network under the form of hybrid couplers, decoupling networks or lumped elements [TPK$^+$11, BYP09, CWC08]. The main drawback of this solution is the loss of bandwidth and efficiency depending on the level of initial coupling between the antennas [LAKM06]. The effect of having a smaller bandwidth can be compensated by introducing a tunable decoupling mechanism as shown in Tatomirescu et al. [TPFP11]. A simple tunable capacitor can extend the operating frequency of the neutralisation line by up to a factor of five. A lumped component feeding network is illustrated as well. However, the number of components and the high insertion loss attributed to them makes this solution undesirable.

For a given geometry, the concept of introducing an extra coupling path to cancel the initial coupling between radiators can be implemented using a several types of scatterers, as illustrated in Andersen and Rasmussen and Lau and Andersen [AR76, LA12]. In Zhang et al. [ZLSH11], two planar inverted-F antenna (PIFA) elements designed for 2.4 GHz are well isolated using a T-shaped slot in the ground plane placed in between the two antennas. The slot enables the design to be very efficient and compact array for a MIMO Wi-Fi application.

There is an asymmetry in demand for uplink data rate versus that of downlink data rates, with higher user interest in download than for upload. Therefore, the classical arrangement in current smart phones is to use MIMO only during downlink communications and utilise only one antenna for uplink communications. In Tatomirescu et al. [TBP13], a scenario with two diversity antennas is investigated. The two dual band folded monopoles are collocated at one end of the PCB to save space in the mobile phone. Because the antennas cover only the receive part of the spectrum, they can be made very compact, and using tunable matching networks, they are able to cover several bands. Although the matching network has only a tunable capacitor and two fixed inductors, matching is achieved over the whole tuning interval for both bands. The low-band antenna correlation is controlled by a simple tunable capacitor in between the elements which controls the backscattered signal thus achieving pattern diversity and a tunable correlation coefficient. Simulations with and without the user in isotropic and anisotropic environments confirm that the initial free space loss is compensated by a lower degradation due to user effect.

In Tian and Lau [TL12], it was shown that six degrees-of-freedom (DOF) can be achieved with a compact co-located array. They are the result of angle and polarisation diversities, as in the case of an ideal E/M dipole array. Further

confirmation is obtained when a larger array is studied. Space diversity is found to contribute significantly to the larger array's effective degree-of-freedom (EDOF) performance. This finding indicates that the space diversity should be exploited whenever possible in array design, in order to complement angle and polarisation diversities and maximise overall EDOF performance, as shown in Figure 10.1. However, the proposed design is only intended to be proof of concept. Implementing the concept practically in the form factor of mobile terminal remains a significant challenge.
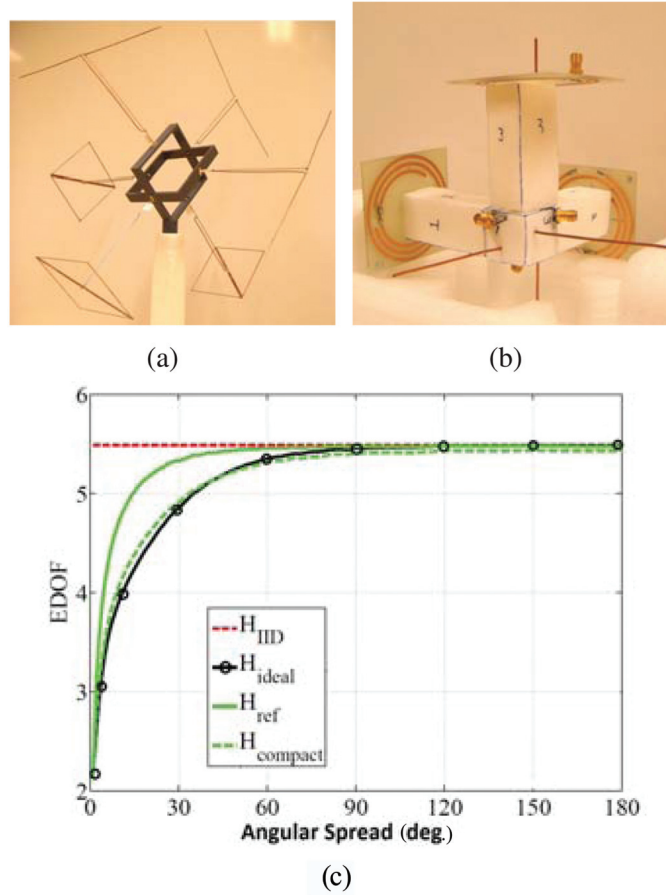

Figure 10.1 Design and evaluation of six-port MIMO antennas: (a) Reference transmit array, (b) compact receive array, (c) EDOF of 6×6 independent and identically distributed (IID) channel **H** and 6×6 channels with ideal, reference, and compact arrays for different angular spreads.

There are some examples in the literature of a topology with both balanced and unbalanced antenna combinations using a fixed [HHG11, IKA$^+$11] or tunable [TAP12] balun. This type of systems has been demonstrated to obtain good isolation. One of the notable drawbacks of this approach is the high Q of the balanced element and the cutback required to minimise the ground plane shorting effect. The narrow-band (NB) operation of the balanced elements can be used for spatial filtering configurations where the Receiver (Rx) and Transmitter (Tx) chains have a dedicated tunable antennas which acts as a duplex filter; this is illustrated in Bahramzy et al. [BSP14]. The work in Bahramzy et al. [BSP14] also investigated the isolation of three antennas in a MIMO mobile handset at 700 MHz, where apart from the isolated Tx and Rx antennas, an additional Rx antenna is added for downlink MIMO. Due to the electrically small structure of the terminal, achieving decoupling among three antennas is a major challenge. Further results on this topic were reported in Bahramzy et al. [BSP15], where decoupling was achieved through the use of a loop antenna and two regular IFAs. This is due to the loop's inherently different electromagnetic properties relative to those of IFAs. One potential practical limitation is that the loop antenna requires some ground clearance.

Recently, full-duplex (FD) systems have attracted a lot of interest in the research community for their ability to allow a radio terminal to transmit and receive simultaneously on the same frequency band. FD systems can potentially double the data rates that can be achieved in half-duplex systems. However, it is very difficult to achieve this in practice due to implementation challenges. Usually, the self-interference (SI) cancellation techniques that were proposed in the prior works use a combination of analog-circuit and digital techniques, or exploit propagation properties [JCK$^+$11, DS10, BMK13]. In Snow et al., Khandani et al., and Aryafar et al. [SFC11, Kha13, AKS$^+$12], the focus is on using the transmit beamforming technique for interference cancellation. Most of these works consider the use of SI cancellation techniques mainly for a single-input single-output (SISO) system [ATTP13]. A natural follow-up is the transmit beamforming approach and an investigation of the feasibility and implementation limitation of the method for a compact MIMO-FD antenna system. In Foroozanfard et al. [FTF$^+$14], an antenna system consisting of six patch elements on the top and bottom layers of a three-layer substrate is proposed, where the transmit antennas are located on the two sides of the substrate and Rx antennas are located in the centre. By arranging the transmit antennas symmetrically from the receive antennas, simple beamforming weights can be applied at the transmit elements to cancel out the SI at the central receiving elements. Antenna polarisation

diversity and spatial diversity is employed to achieve higher isolation between different ports. The results show a significant amount of cancellation within the range of 60–75 dB. A different antenna setup is investigated in Foroozanfard et al. [FdCP14], where three dual-polarised patch antennas are mounted on the ground plane and radiate in the same direction. Furthermore, the investigation on the effect of the implementation accuracy on the system performance came to the conclusion that passive transmit beamforming is very sensitive to antenna misalignment. However, to remove the sensitivity of the antenna misplacement, active beamforming can be used to adapt the system to the impairments and also any reflection from the environment. This method can be a potential solution for achieving high-SI cancellation where the price is having redundant antennas.

10.2.1.1 Other antennas for high data rate systems

MIMO systems have been adopted in many mobile communication systems. However, the current throughput of MIMO systems will not permanently accommodate the data rates needed by individual users and operators. In an effort to support the growing data rates and to understand the limitations of both MIMO and massive MIMO systems, the characterisation of multiple links is becoming increasingly more important. In order to measure multiple links accurately, a three-dimensional array which is capable of measuring both polarisations is necessary. In Müller et al. [MKH$^+$14] this type of array was built, tested, and optimised for high-resolution parameter estimation. Other efforts have focused not on the channel but on combining UWB and MIMO for significantly increasing total throughput. Achieving this type of system is difficult as each pair of antennas in the UWB MIMO system must maintain a low envelope correlation coefficient (ECC) across the entire frequency band. In Zhang et al. [ZLSH12], a 3.15- to 5.15-GHz two element MIMO universal serial bus (USB) dongle was developed which maintained an ECC of below 0.1 across the entire band. If data rate trends continue, massive MIMO UWB systems may become the standard for high data rate mobile communication systems. In these systems the channel must be well characterised in order to obtain the benefits of both systems.

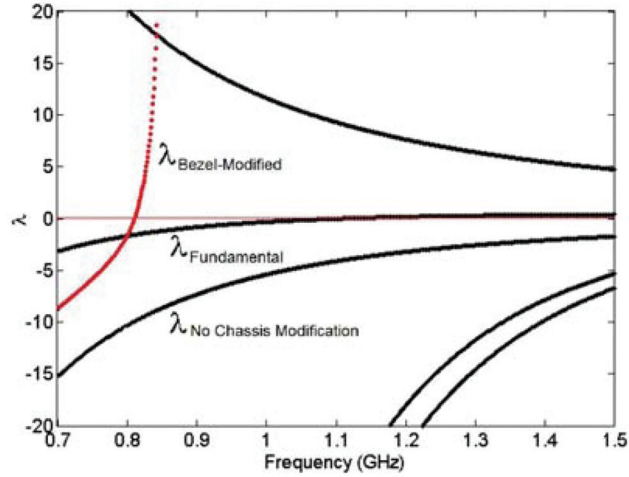### 10.2.2 MIMO Terminal Antennas with Characteristic Modes

The challenges of implementing efficient antennas within small mobile terminals have dramatically increased due to the adoption of MIMO technologies. MIMO systems require implementing multiple antenna elements that are

packed into a single electrically small volume. Designing antennas in this type of systems becomes challenging due to the close proximity of radiating elements which will strongly couple to one another.
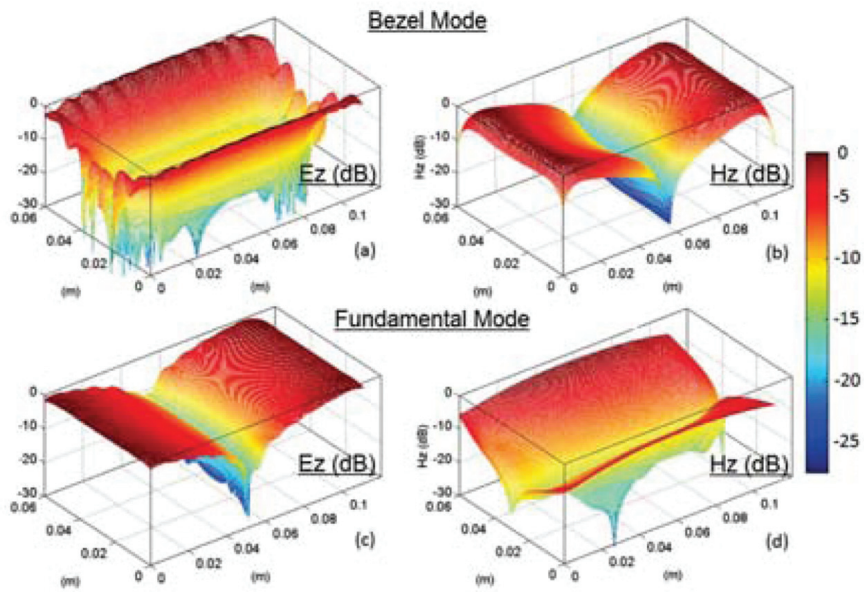
Numerous techniques have been proposed in the literature to mitigate coupling between antenna elements but relatively little attention has been given to the problem of chassis induced coupling, TCM provides solutions to this problem. TCM is based on the generalised eigenvalue equation $X J_n = \lambda\ R J_n$, which is derived by optimising the far-field radiation of a given structure. This equation is often solved using the method of moments (MoM) impedance matrix (i.e., $Z = R + jX$) and when solved provides the currents J_n for each orthogonal far-field which a structure is capable of radiating [HM71].

Initial work done through designing MIMO antennas based on TCM proved it is possible to understand the fundamental characteristics of a mobile chassis and why it is difficult to obtain both wide bandwidth and low correlation among multiple elements. The fundamental characteristic modes of a candy bar style mobile phone can be solved for using TCM and are shown (black) in Figure 10.2(a) [LML13]. For this type of chassis there is only one resonant mode below 1.5 GHz ($\lambda_{\text{Fundamental}}$) which is referred to as the fundamental mode. It should be noted that a mode is resonant when it has an eigen value of zero, if the eigenvalue is negative or positive this indicates that the mode is reactive. The more capacitive or inductive a mode is, the higher quality factor the mode will maintain, and thus when properly fed, will have a maximum bandwidth as set by the quality factor.

Characteristic modes can be utilised to reduce the mutual coupling between multiple antennas on a mobile chassis. An example of this concept was described in Li et al. [LLH11], where it was shown that a single antenna on a chassis can be used to exploit the fundamental chassis mode, whereas a second antenna can be designed to avoid chassis excitation. This same idea was further expanded upon in Li et al. [LLYH12] by co-locating an electric antenna with a couple fed magnetic antenna. This enabled having two fully decoupled antennas while adhering to industry accepted antenna size constraints. The magnetic antenna, which did not couple to the fundamental mode, was fed using a magnetic loop consisting of two half square rings, while the fundamental mode was fed using a standard electric monopole antenna. In this same work it was shown that the TCM-based design is capable of providing nearly optimal MIMO performance. This analysis has been done by comparing the capacity of the TCM designed antenna against both the ideal capacity and the capacity of a typical monopole/PIFA antenna configuration. The channel capacity for the three cases were calculated and presented in Li et al. [LLYH12].

(a)

(b)

Figure 10.2   (a) First five characteristic modes of flat chassis (*black*), modified bezel mode (*red*). (b) Near-fields of fundamental and bezel modes.

In Li et al. [LLYH12], it was shown that performance increase can be obtained when using TCM as a way to decouple antennas. However, this led to reduced bandwidth and the designed system could not be used for LTE operation, unless the narrowband magnetic antenna can be tuned on demand. Nevertheless, Li et al. [LML13] and Bouezzeddine et al. [BKS13] describe a new design methodology which is based on utilising TCM to develop new modes in a structure which then can be excited. This design approach relies on manipulating the chassis so that more than one characteristic mode is resonant at the frequency of interest. To illustrate this design concept, the authors of Li et al. [LML13] added a metallic bezel to the terminal casing. When this bezel structure is analysed using TCM a new mode becomes resonant below 1 GHz as is shown in Figure 10.2(a) in red, where λ_{Bezel} is the new bezel mode, $\lambda_{\text{Fundamental}}$ is the fundamental mode, and $\lambda_{\text{No Chassis Modification}}$ is no longer present. This new mode is orthogonal to the fundamental chassis mode and as such when the far-field ECC of the two modes is calculated the result is 0. In the companion work of Miers et al. [MLL13] it was shown that through the use of TCM near-fields and currents it is possible to pinpoint possible feeding locations which can excite one mode without coupling into the other mode. The bezel mode was fed using the characteristic reactive near-fields seen in Figure 10.2(b). On either of the short edges of the structure the bezel mode has high-magnetic field strength and the fundamental mode has high-electric field strength. If an electric and magnetic feed elements are placed at this location the magnetic element will feed the bezel mode while the electric element will feed the fundamental mode.

It is possible to use TCM to manipulate a structure to support multiple resonances, as done in Miers et al. [MLL14]. This is applied by cross correlating the area around the feeds with the currents and near-fields of higher frequency modes. Using this information it is possible to determine what modifications to a structure can produce uncorrelated resonances at multiple frequency bands. In the structure described in Miers et al. [MLL14], the authors accomplished this by introducing a small HF resonant structure to create a new mode which the low-frequency feeds excite at higher frequencies.

The application of the TCM is not restricted to small wireless devices but can be extended to larger structures equipped with more than two antennas. The system considered in Bouezzeddine et al. [BKS13] and Bouezzeddine and Schroeder [BS14] was designed to be used as a four-port MIMO customer premises equipment (CPE) antenna system for operation in TV white space bands. Characteristic mode analysis of the chassis of the device was applied

to determine location and types of couplers for excitation of four mutually orthogonal superpositions of characteristic modes. A four-port antenna system with high isolation was obtained.

Designing efficient antennas through the use of TCM is not confined to the types of systems described above, many other systems have been designed using this method including, but not limited to, vehicular [IF14], mmW [BVV+14], and dielectric resonant [AEM14] antennas.

10.3 Reconfigurable and Channel-Aware Antennas

With their increasing functionality, mobile phones are embedding better screens, better cameras, larger batteries and more antennas, among others. In order to keep the portability of such devices, a high degree of integration is needed. Section 10.3.1 discusses frequency-reconfigurability as a miniaturisation technique. Moreover, the effects on the antenna total efficiency are investigated. However, when assessing the performance of multi-antenna systems, the efficiency alone cannot provide enough insight into the handset performance. Section 10.3.2 relates the antenna characteristics to the propagation conditions, via the channel capacity. Channel-aware antennas are considered, they evaluate the channel and accommodate to it in order to enhance the capacity.

10.3.1 Frequency-Reconfigurable Antennas

Chipset miniaturisation has seen a large success over the last years. However, antenna volume is ruled by fundamental laws that relate size, efficiency, and bandwidth. To support the latest mobile communication standards, LTE and LTE-Advanced (LTE-A), antennas need to operate in frequency bands ranging from 698 MHz to 2.690 GHz. Tunable antennas are a very promising way to reduce antenna volume while enhancing its operating bandwidth. Tunable antennas use a tunable component in order to reconfigure their resonance frequency. These antennas exhibit an instantaneous narrow bandwidth, that can be reconfigured to a wide range of frequency, thus resulting in an effectively wide bandwidth.

10.3.1.1 Loss mechanism of frequency-reconfigurable antennas

A system using tunable antennas offers a better interference rejection due to the NB nature of the system, leading to relaxed specifications on channel select filters, e.g., SAW filters. Fornetti et al. [FSHB12] uses antenna tuning to increase the handset efficiency and sensitivity. Hence the reliability of the

wireless data link and the battery life are enhanced and the pressure on the infrastructure is decreased. A tunable antenna has been built using digitally tunable capacitors (DTCs) provided by Peregrine semiconductors to address LTE bands at 1.7 GHz. These designs exhibited a large amount of loss. However, it must be noted that the loss of performance introduced by the tunable antenna may be acceptable at system level and lead to an overall increase in transceiver performance, hence bringing economical advantages.

The work by Del Barrio et al. [DBPFP12] focuses on the impact of the tuner loss on the efficiency of NB antennas, depending on the location and capacitance of the tuner. The results indicate that different combinations of added capacitance and tuner location can lead to the same resonance frequency, but different losses and required capacitance range. Measurements show a loss difference of 1.2 dB between different combinations of location and capacitors, at the same resonance frequency.

Del Barrio et al. [DBMP14] uses a capacitively-loaded handset antenna and a MEMS tunable capacitor from WiSpry [WiS]. This paper highlights the importance of co-designing the tuner and the antenna to optimise radiated performance. A prototype is shown in Figure 10.3(a), where the antenna volume is 0.5 cc. Its tunability in the low-LTE-bands is shown in Figure 10.3(b). The antenna is highly sensitive to the insertion loss of the tuner, due to its high antenna quality factor. The measured total efficiency decreases as the antenna is tuned towards lower frequencies. It has been noted that the tuner loss is not the only source of loss. The metal loss due to non-perfect conductor (i.e., copper) is significant for a high-quality factor antenna. Thermal loss is inherent to the antenna manufacturing and draws a limit to the achievable performance of tuned antennas.

Simulations of two planar handset antenna designs addressing the low-bands of LTE are presented in Tatomirescu et al. [TAP13]. They are frequency-reconfigurable but differ by their quality factor (Q). The tunability is enabled
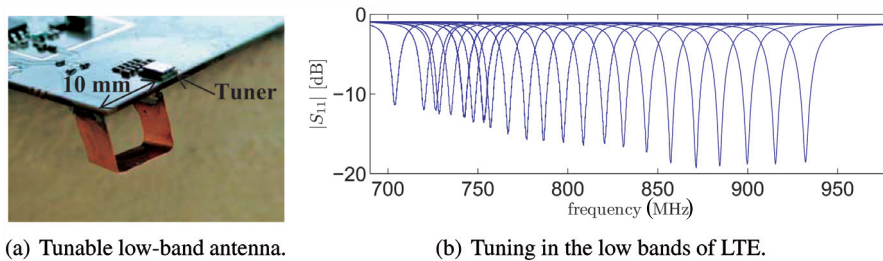

(a) Tunable low-band antenna.   (b) Tuning in the low bands of LTE.

Figure 10.3   Frequency-reconfigurable antenna for LTE mobile phones [DBMP14].

using a MEMS tunable capacitor. For MIMO purposes, the antenna design is duplicated and placed on the same board. Five different placements of the secondary antenna are investigated. The results show that isolation between antennas is improved by using NB elements. Moreover, antenna placement on opposite sides of the PCB achieves a high level of isolation, even when the antennas are tuned to 700 MHz. In spite of the lower radiation efficiency that high-Q antennas present, their overall performance is better than the low-Q antennas, due to their inherently reduced coupling.

Due to the popularity of tunable antennas, the demand for manufacturing cost reduction is stronger than ever. Hence, Buskgaard et al. [BTDBP15] looks into manufacturing of antennas using a silver-based conductive ink on a plastic foil, which is a very cost efficient way of producing antennas, because it is possible to mass produce antennas onto a big roll of foil. For low-Q antennas the process looks feasible. However, high-Q antennas, because of the high currents, are extra sensitive to the sheet resistance of the metal used. The measurements show that the efficiency is much worse for the printed high-Q antennas than for a copper reference antenna.

10.3.1.2 NB tunable Tx and Rx antennas for a duplexer-less front-end

Conventional FD radio communication systems require that the radio Tx is active at the same time as the radio Rx. The increasing number of frequency bands require either a bank of NB filters with a switch or agile duplexers. While practical agile duplexers are not available, a bank of narrow-band filters with a switch is bulky and incurs switching loss. A novel front-end architecture, addressing the increasing number of LTE bands as well as multiple standards, is shown in Figure 10.4(a). NB antennas are used in order to provide sufficient rejection between the Tx and Rx. The investigation by Bahramzy et al. [BJSP14a] compares loaded antennas, capacitively and inductively. The inductive kind exhibits a smaller antenna volume for a given Q, where the inductance tuning is done with an LC circuit. A complete front-end [BOM$^+$14] has been designed and fabricated to demonstrate the performance of the proposed architecture, where each component, including tunable antennas from Bahramzy et al. [BJSP14b] (Figures 10.4(b,c)), are designed specifically to fulfill the system requirements.

An alternative method for obtaining duplex function is described in Laughlin et al. [LZB$^+$15]. This technique is about exploiting electrical balance (EB) in hybrid junctions to connect the Tx and Rx chains to a shared antenna, while providing high isolation between them. High Tx–Rx isolation can only
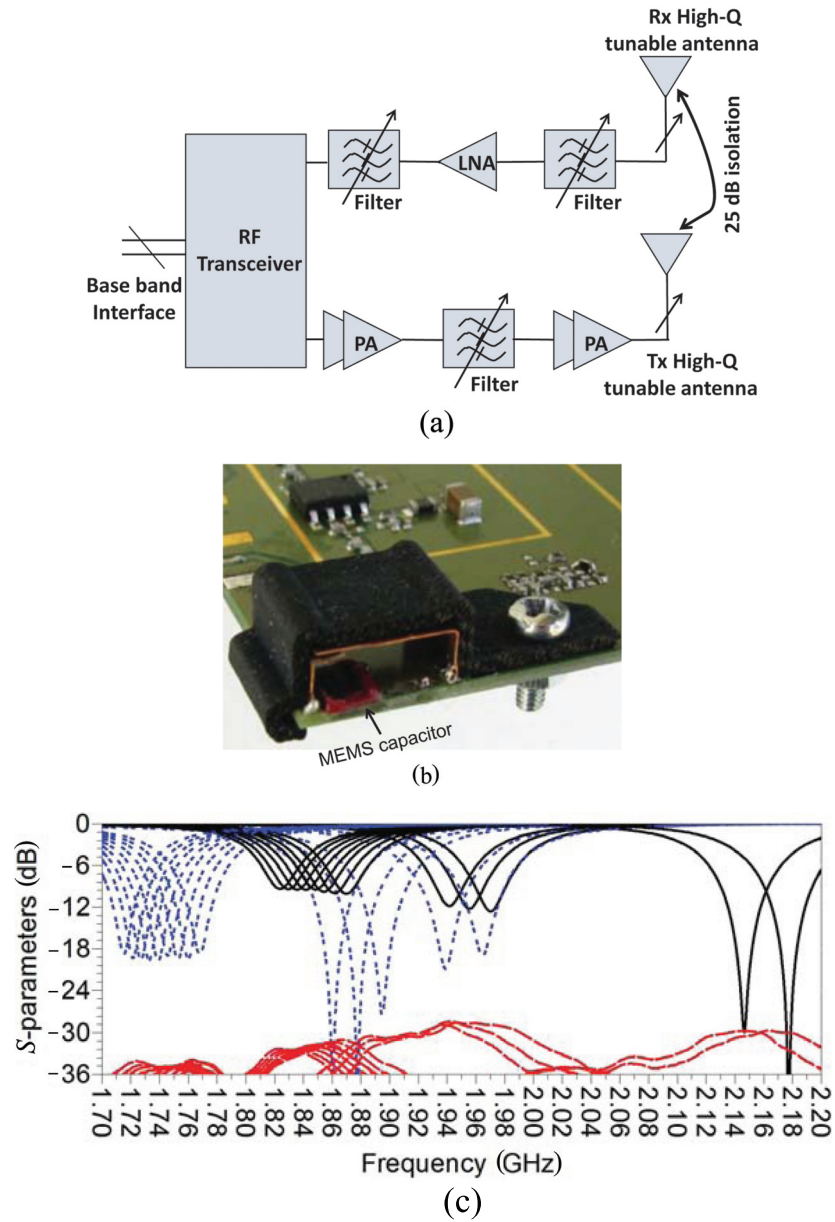
(a)

(b)

(c)

Figure 10.4   (a) Front-end with no duplex filter, (b) close-up of the antenna, and (c) measured scattering parameters of Tx and Rx antennas.

be acheived when the antenna impedance is closely matched by the balancing impedance, and the typically divergent nature of the antenna as well as the balancing impedances limits the isolation bandwidth of the EB duplexer. EB duplexing alone cannot provide the neccesary level of analog cancellation required for full duplex operation. However, when combined with active Analog Cancellation (AC), more than 80 dB Tx–Rx isolation is achievable over a 20 MHz bandwidth.

For LTE bands below 1 GHz, mobile phone antenna performance strongly depends on the ground plane size. Tatomirescu and Pedersen [TP14] shows how NB tunable antennas, due to their high-Q nature and thereby confined near-fields, can be somewhat ground plane size independent. The proposed tunable PCB antenna comprises two elements, occupies an area of 10×30 mm^2 and satisfies requirements of carrier aggregation combinations through NB dual-resonator design. With PCB size variation from 130×65 mm^2 to 70×50 mm^2, it is noted that impedance match and bandwidth stays reasonably stable.

10.3.2 Channel-Aware Antenna Design

For MIMO operation, LTE requires multiple antennas to be deployed at both the Tx and Rx. This requirement provides significant benefits in terms of higher data rates and better link reliability, but it also imposes significant challenges on antenna designers: (i) multi-antenna elements distributed within a compact volume increase the likelihood of the antenna elements being detuned by a user; (ii) the MIMO performance of multi-antennas (e.g., channel capacity) does not only depend on the received power, but also on correlation, which is a function of the antenna patterns and propagation channel characteristics.

10.3.2.1 User effect compensation for terminals with adaptive impedance matching

Adaptive impedance matching (AIM) can provide large performance enhancements in the presence of users, compared to free space operation. Apart from compensating for the detuning of an antenna caused by user proximity, adaptive matching also introduces a degree of frequency-reconfigurability for covering an increasing number of operating bands.

A dual antenna system is investigated in Plicanic et al. [PVTL11] and Vasilev et al. [VPL13], where the potential MIMO capacity gain from adaptive matching is examined in Plicanic et al. [PVTL11]. The *S* parameters were measured in an indoor office environment, with the terminal held by phantom

hands. Ideal adaptive matching circuits were then added in post-processing. From the capacity performances with and without matching in the NLoS scenario at 0.825 GHz, it is observed that optimal matching for the two hand case enables a large capacity enhancement of 44% at 50% outage probability relative to no matching, which is mainly due to increased received power. The potential of AIM in the 0.8 GHz band based on two fabricated MIMO terminal prototypes (A and B) of significantly different antenna properties is also investigated [VPL13]. Prototype A has good impedance matching but poor isolation and NB behaviour, whereas prototype B has poor matching but high isolation and wide bandwidth. Assuming a reference signal-to-noise-ratio (SNR) of 20 dB, the capacity gain for prototype A is very high in the two-hand case, suggesting that AIM can significantly improve the capacity performance in cases where there is severe antenna mismatch. The performances of three dual-antenna terminals with adaptive matching were evaluated under four different user scenarios [VFL13]. It was observed that the prototype with the smallest antenna bandwidth and largest isolation can benefit the most from adaptive matching in the presence of a user (i.e., 24% capacity gain), which is because the adaptive matching networks effectively compensate for user-induced detuning.

The benefits of AIM, in compensating for performance degradation from propagation channel and user effects is studied in Vasilev et al. [VPTL13], based on field measurements. A MIMO terminal prototype equipped with either two ideal matching networks or two mechanical tuners was measured in three user scenarios and two propagation environments, see Figure 10.5. It was found that, due to the relative position between the hand and the terminal
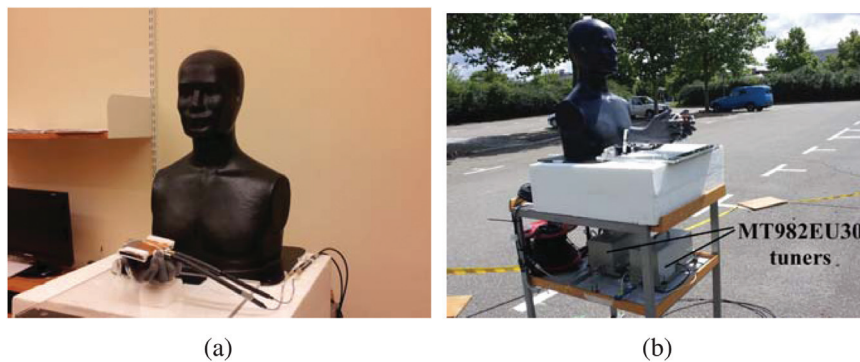

<center>(a)   (b)</center>

Figure 10.5   Channel measurement Rx setup: (a) Indoor scenario with one-hand grip and (b) outdoor scenario with two-hand grip, with MT982EU30 tuners shown [VPTL13].

antennas, the mismatch and therefore capacity gains in the one-hand cases were significantly lower than those in the two-hand cases. Further, since the user effects are less severe in the high band, the capacity gain is only up to 8% for these cases.

10.3.2.2 Channel adaptation to enhance capacity and localisation

UWB detection is an attractive solution for low-cost radar and localisation in the far field, while medical imaging has used UWB in the radiating near field. An understudied use of UWB is the possibility to apply detection methods in the sensors' reactive near field, where initial studies have been carried out in Ma et al. [MBH13]. The detection of eggs in a smart fridge is chosen as a case study. Exhaustive measurements have been carried out using an array of UWB sensors illustrated in Figure 10.6 where the filtering effect due to the presence of an egg can be quantified regardless of position by evaluating the maximum group delay of the UWB impulse or using a newly derived correlation coefficient when an egg is on top of the sensor. It is assumed the egg box is used and its presence above the sensors is known. The presence of clutter in the fridge such as the tomato in Figure 10.6 is also considered. Such concepts can be reliably implemented in smart container and packaging applications, where the sensors are invisible when fabricated with graphene or carbon nanomaterials.
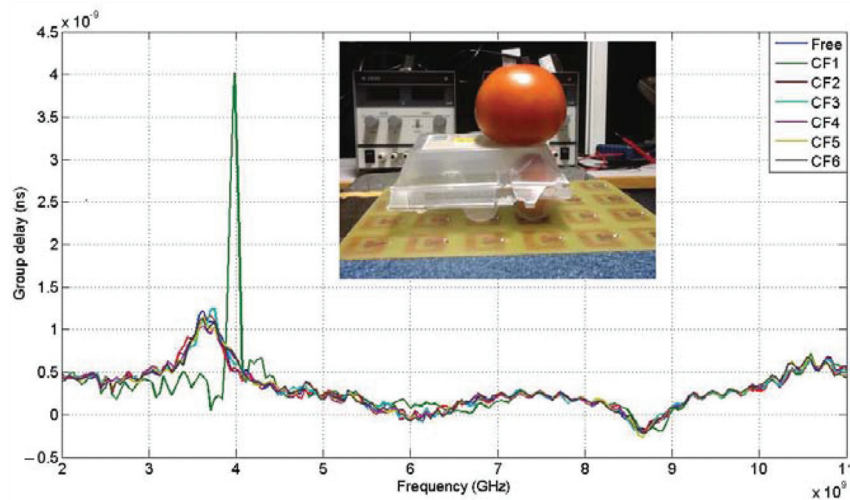

Figure 10.6 Frequency responses for the test case scenario of reactive near field UWB egg detection, when an egg is placed over a sensor [MBH13].

MIMO systems require a high degree of complexity due to the necessity of multiple radio-frequency (RF) chains. An adaptive reconfiguration of basis patterns in both Tx and Rx creates the possibility of reducing the transceiver complexity and provides the ability to design very small MIMO capable devices. In Vasileiou et al. [VMTK13], electronically steerable passive array radiators were used for beamspace MIMO systems. Previous work used these arrays with a specific set of basis patterns, in order to obtain a spatial multiplexing scheme for multiple data streams. This ensures orthogonal transmission of multiple data streams, though only in ideal channel conditions. The work in Vasileiou et al. [VMTK13] considers the variations of the channel and proposes to adaptively select the most effective basis pattern for the Tx and Rx sides. The goal is to diagonalise the beamspace channel matrix and ultimately to maximise the system capacity. This is done by developing channel-aware basis pattern calculations, which are based on SVD factorisation. The main contribution of the work is to propose a solution that works under realistic conditions. The work outperforms the current state-of-the art techniques, which do not take into account the channel, as can be seen in Figure 10.7.

Author Narbudowicz et al. [NAH15] propose a compact pattern-reconfigurable antenna design for femto-cell base station application. The advantages of the design are two fold: the direction of the beam can be continuously steered within 360° using phase shifting and the steering can
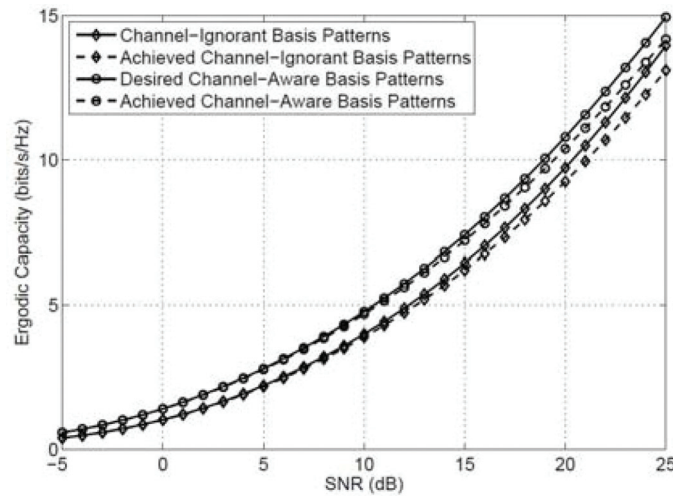

Figure 10.7   Achievable ergodic capacity using the channel-ignorant versus the channel-aware basis patterns [VMTK13].

be controlled by the modulation scheme. Consequently, the design allows independent steering for each channel. Applications of the proposed antenna tuning concept can be extended to wireless local area network (WLAN) access points, sensor networks or even enhanced localisation support.

The work by Li and Lau [LMCL15] present a pattern-reconfigurable antenna design for mobile phone application. The investigation is carried out on the low bands of the 4G spectrum, which is a real challenge since the chassis is the dominating radiator at these frequencies. The design is based on the characteristic mode analysis of a bezel-loaded chassis and uses PIN diodes to switch between the states. Simulations show patterns providing an envelope correlation below 0.2 within the investigated frequencies.

In Glazunov and Zhang [GZ11], the interactions between the propagation channel and the antennas are discussed in a MIMO context. A unified approach to characterise such interactions is proposed, using both the spherical vector wave expansion of the MIMO channel and the scattering matrix of the antennas. This method provides a better insight into the behaviour of the radio propagation channel, and helps characterising throughput and channel correlation, among others. The goal of the work is to obtain uncorrelated antenna radiation patterns, in order to achieve the specifications of LTE systems. The contribution shows that the spherical vector wave coefficients of the transmit antenna are the eigenvectors of the multi-mode correlation matrices at the transmitting antenna. The same conclusion is valid for the receiving antenna.

A previously developed synthesis method for NB antennas is extended to UWB antennas by Sit et al. [SRL$^+$12]. The method maximises the capacity by tuning the patterns of the MIMO antenna system. This proves to be challenging since the channel characteristics change over the large UWB spectrum, hence affecting also the radiation pattern and the orthogonalisation process. The synthesis method aids in reducing the number of antenna elements needed in the final antenna system. In this paper, the resulting optimal radiation pattern for an indoor scenario is shown and the capacity analysis is also presented.

10.4 RFID and Sensor Antenna Innovations

This section highlights novel ideas in the research area of RF Identification. The trends for future applications are towards smart antenna research, where more functionality is introduced in the RFID chip cards as well as in the antennas for RFID readers. The miniaturisation of antennas is the key driver for the research on tags and wireless sensor nodes.

10.4.1 Antennas for RFID Readers and Chip Cards

A smart antenna at the reader side of an RFID system is presented in Lasser et al. [LMPM15]. The horizontally polarised, azimuth switched-beam antenna is designed for novel RFID-based tyre pressure monitoring systems in vehicles. The intended mounting position is below the body floor pan, which usually constitutes a large conducting object. To maintain the efficiency and pattern properties of the switched-beam antenna, the authors of Lasser et al. [LMPM15] use a dual-band frequency selective surface (FSS) manufactured from printed circuit boards mounted between the antenna and the body floor pan (Figure 10.8). This surface is designed to reflect a plane wave without phase shift and, therefore, enables efficient operation of a close-by antenna. An efficiency penalty of just 0.8 dB is measured at 868 MHz for a small FSS panel of 0.87 λ_0 edge lengths closely spaced at 0.08 λ_0.

A smart active UHF RFID tag is proposed for the use in a warehouse scenario in Dufek [Duf12]. Equipped with an adaptive antenna array, the tag is able to steer its beam towards a reader station using phase shifters embedded in the substrate. This system is considered advantageous for example in warehouses, where the to be tracked goods are moving, or if interferences are present due to multipath propagation. In addition to that, the communication range can be extended.

For designing contact-less chip cards and HF tags for various application scenarios, a good model of both the coil antenna and the RFID chip are necessary to match both components perfectly for an efficient power and data transfer. In Gvozdenovic et al. [GPM14] a planar spiral inductor synthesis method is discussed, which generates physical dimensions of an HF RFID
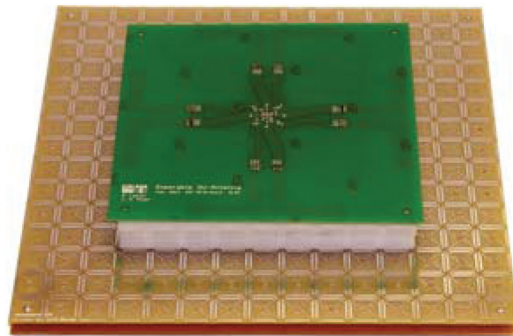

Figure 10.8 Photograph of the switched-beam antenna mounted atop the FSS using foam spacers for a spacing of 28 mm [LMPM15].

antenna according to specified equivalent circuit parameters. A numerical model for a spiral coil based on the partial element equivalent circuit (PEEC) method is combined with a non-linear optimisation algorithm to optimise and synthesise coils. The PEEC engine is implemented in Matlab and the inductance values of the synthesised circular spiral coils are comparable with the simulation results obtained from commercially available 3D EM simulators as well as with measurements [GMP+13]. In Gvozdenovic et al. [GMM14] the non-linear behaviour of an RFID chip is evaluated by measurement and described by a simplified harmonic model. A manual for designing HF RFID tags is created which includes a procedure for measuring the impedances of coil and chip, and simple fitted formulas for quick calculation of coil parameters in order to achieve required resonance frequency and bandwidth.

10.4.2 On-Chip Antenna Design for Miniature RFID Tags

To decrease the size of an RFID tag dramatically (some mm^2) and to reduce the overall manufacturing costs, the metallisation layers of a cost efficient 130 nm CMOS process are utilised for antennas operating below 10 GHz. An UWB-pulsed data stream is considered in the uplink from the tag to a reader once the tag is powered and controlled via an UHF signal, forming an asymmetric or hybrid communication scheme. The addition of UWB into a tag introduces a substantially increased data rate, while compatibility to standard UHF reader is kept. Towards such a system, several compact on-chip antennas (OCAs) with a size of 1 mm^2 such as loops, dipoles and monopoles on a CMOS substrate are designed, manufactured and analysed to investigate the different communication links [GSM13].

A CMOS testbed, consisting of a circuitry and an OCA on the same die, has been manufactured [GWHM11] to investigate the UWB communication. This is considered critical, because the large Q-factor of ESAs limits the maximum achievable bandwidth. The circuitry features a voltage controlled oscillator, selectable data sources, a bandwidth adjustable glitch generator for a pulse amplitude modulator and a power amplifier. A horn antenna was placed 60 mm above the device, which was able to capture the wideband PAM signal. In Gvozdenovic et al. [GGM11], an antenna array is proposed to increase the gain at the reader station and to roughly localise the tag. Depending on the centre frequency and the embedded OCA type a large radiated bandwidth is measured, which can be explained that the efficiency of the OCAs is low, due to the small size of the antenna and the losses introduced by the silicon substrate and, therefore, the Q-factor is lowered as well. The measured

bitrate is up to 100 Mb/s. With this technique a detailed characterisation of the radiated field of the manufactured on-chip antenna types is presented in Gentner and Mecklenbräuker [GM11]. In Gvozdenovic et al. [GGM12], a near-field channel from the actively powered UWB RFID tag with an OCA is measured and a simple channel model is proposed. The measurement and characterisation of a tiny tag with OCA is best done without any mechanical connection (bondwires). This is necessary to avoid any mutual coupling between the measurement feed connection, which can blur the measurement results by an angular tilt of the radiation pattern [GASM12].

A miniature UHF/UWB hybrid silicon RFID tag is presented in Gentner et al. [GLS$^+$13]. This system-on-a-chip (SoC), shown in Figure 10.9, features two OCAs for an asymmetric communication. By inductive coupling, energy is received by a loop OCA and stored in a buffer capacitor on-chip. The tag receives control commands via the UHF link established with the loop, and transmits a 10 μs long hardcoded 4-PPM stream with the monopole OCA. This data stream, with a datarate of 117Mb/s, has been successfully captured and analysed for a measurement distance of 5 mm.

10.4.3 ESAs for Wireless Sensors

The design of a circular inverted-F antenna (CIFA) by Kakoyiannis and Constantinou [KC12b, Kak14] demonstrated that the exploitation of the circumscribing sphere of a wireless sensor to the greatest possible extent is the most effective miniaturisation technique, even for planar/printed (2-D)
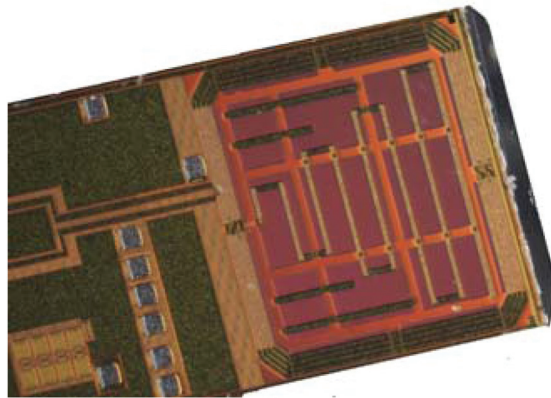

Figure 10.9 Micro-photograph of the on-chip antennas of an UHF/UWB hybrid silicon RFID tag. This tag has a size of 3.5 mm × 1 mm.
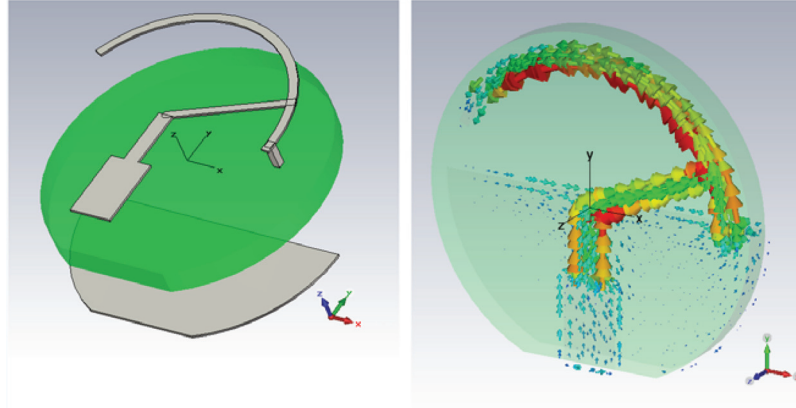
Figure 10.10 Layout and current density of a CIFA antenna. Picture published in Kakoyiannis and Constantinou [KC12b].

antennas. By shaping the radiating part of the current distribution into a circle close to the boundary, an ESA of size $ka = 0.5$ rad is obtained at 2.5 GHz with a 3.5% BW and a 90% efficiency (see Figure 10.10). The antenna is based on a minimal design space (two angles and a radius) and features a wide tuning range by way of modifying one or both angles. Based on first principles, the system model of the CIFA naturally leads to an upper bound on the directivity of ESAs. The upper bound can be tight or loose, depending on the shape of the current distribution. If efficiency proves to be high, then this bound also becomes a tight upper bound on the gain of ESAs. Finally, based on reasonable assumptions regarding the equivalent circuit at the input to the CIFA, a minimum transmission frequency for ever-shrinking sensor nodes can be derived. A forecast model predicts that Smart Dust nodes need to enter deep into the mmW region (approx. at 42 GHz), if they were to use microwaves for wireless communication.

10.5 Modelling and Characterisation of Antenna Systems

As an important component of wireless communication, an antenna is never independent from its surroundings, i.e., the propagation channel. Modelling and characterising antennas in a systematical way is very important, taking into account system performance and channel influence. In Section 10.5.1, multiplexing efficiency is introduced as a system metric for convenient evaluation of MIMO antenna performance. After that a simple method to

measure the signal correlation of MIMO antennas is illustrated, followed by statistical antenna pattern analysis and pattern interpolation for use in channel modelling and emulation. The antenna system is analysed in real conditions in Section 10.5.2, including the factors of mobile devices, the mobility of the terminal and the real propagation scenario. The discussion is then continued into the interaction between users and antennas in Section 10.5.3, where hand, head and body are all taken into account.

10.5.1 Methodologies and Modelling

MIMO technology has been widely introduced in wireless communications due to its ability to increase the data rate linearly with the number of antennas, without any additional expense in transmit power or spectrum. To characterise the system performance of a MIMO link, several figures-of-merit (FOM) have been proposed, such as channel capacity and diversity gain, which take into account both the antenna and propagation effects. However, those figures cannot provide intuitive information to antenna designers regarding the impact of individual antenna design parameters. To address the effect of antenna parameters on MIMO performance, multiplexing efficiency was introduced [TLY11], which is a power-based metric.

Multiplexing efficiency is defined as the power penalty of a non-ideal antenna system in achieving a given capacity, compared with an ideal antenna system with 100% total antenna efficiencies and zero correlation among the antennas. Assuming that there is no correlation at the Tx and the receive antennas being the MIMO antennas under test, the multiplexing efficiency for a $M \times M$ MIMO system at high SNR can be approximated by

$$\eta_{\text{mux}} = \left(\prod_{i=1}^{M} \eta_i \right)^{\frac{1}{M}} \det(\bar{\mathbf{R}})^{\frac{1}{M}} \qquad (10.1)$$

where η_i is the total efficiency of the ith antenna port, and $\bar{\mathbf{R}}$ is a normalised correlation matrix whose diagonal elements are 1 and off-diagonal element denotes the complex correlation coefficient between the 3D radiation patterns of the antenna ports. In Equation (10.1), the efficiency imbalance and correlation between the antennas are translated to an equivalent power loss in decibel (dB). Based on the separate contributions from the antenna efficiency and the correlation, multiplexing efficiency can also be used to clearly explain the total impact of the user on MIMO terminals [TLY12]. This insight allows antenna designers to effectively quantify and address key parameters in designing MIMO terminal antennas for typical usage scenarios.

As shown in Equation (10.1), signal correlation among the antennas is a critical parameter for the MIMO performance. The conventional way of measuring the correlation is time-consuming, costly and needs specialised measurement facilities [Cla96], which requires information of phase and polarisation. To simplify the correlation measurement, a method based on equivalent circuits was introduced in Li et al. [LLLH13] for estimating correlation coefficients in lossy antenna arrays accurately. The idea is described as a cascade network model in Figure 10.11. A lossy dual-antenna array is equivalent to a network consisting of a lossless circuit in series with loss resistors, which represent the conduction and dielectric losses of the antennas. The value of the resistance r_{loss} can be calculated with the dual antenna circuit model with the knowledge of antenna efficiency. With the information of S parameters of the lossy array and the resistance, the correlation coefficient of the lossy array can then be calculated from the S parameters of the equivalent lossless circuit using the closed form expression from [BRC03]. The method requires only S parameters and antenna radiation efficiencies, with the latter being easier to acquire than radiation patterns. Detailed examples on how to estimate the correlation for dipole antennas were provided in Li et al. [LLLH13], and the method can be extended to calculate correlation for more than two elements.

To design high-performance MIMO antennas with low correlations, orthogonal or quasi-orthogonal radiation patterns are required. Fortunately, TCM provides a convenient tool for MIMO antenna design, as it enables orthogonal radiation patterns to be excited in a given antenna structure. However, eigenmodes solved from the MoM impedance matrix [HM72] are not always maintained across the frequency points, as some modes can
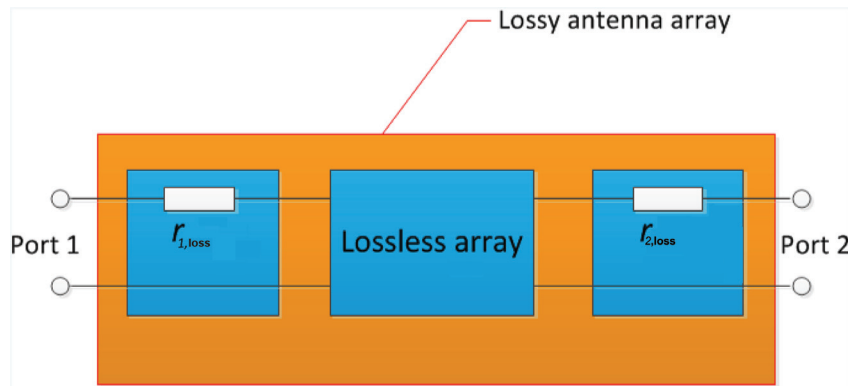

Figure 10.11 Cascade network of a dual lossy antenna array.

become unstable and cease to exist, whereas other modes can appear and become stable without having any relation to previous modes [CHHE11]. An improved method to track the mode based on far field patterns was presented in Miers and Lau [ML14]. This method is based on the fact that the far fields remain relatively stable with respect to variations in structural complexity and frequency. Since the eigen-far-fields are orthogonal to one another, every individual mode is unique and has no correlation to any other mode. By applying the standard multi-antenna ECC equation [VTK10] to modes at different frequencies, the modes with high correlation at different frequencies are successfully tracked as the same mode.

The antenna in real channel realisation is important for practical reasons. The antenna-channel joint modelling of multiple antenna terminals in a wireless communications context was carried out in Sibille [Sib15]. The research is based on the generation of a finite set of data, which represents the terminals characteristics and exploits the existing propagation channel models. In the paper, low-pass filtered antenna patterns are used to exploit the angular structure of the propagation scenario, and complex spatial correlation stemming from the angular dispersion of the propagation was accounted by using the full set of discrete DoA. In this way, the model is simplified with a limited set of parameters. For channel estimation purpose, the complex response of the embedded antenna must be known for all angles of incidence. As the antenna pattern is measured at discrete angles, interpolation is needed. A simple and fast method to characterise, compress and embed antenna patterns is introduced in Kotterman and Landmann [KL12] using effective aperture distribution function (EADF). A critical step in the method is to make the measured pattern periodic, so that the EADF can be applied. For measurements in spherical coordinates, the azimuth direction is periodic by nature, and periodicity in elevation is achieved by concatenating measurements from two opposing meridians, as were the measurements taken along one great circle on the measurement sphere. By performing an inverse 2-D discrete fourier transform (DFT) on the EADF for those particular values of azimuth and co-elevation pairs, a compact representation of complex antenna patterns are achieved after interpolation.
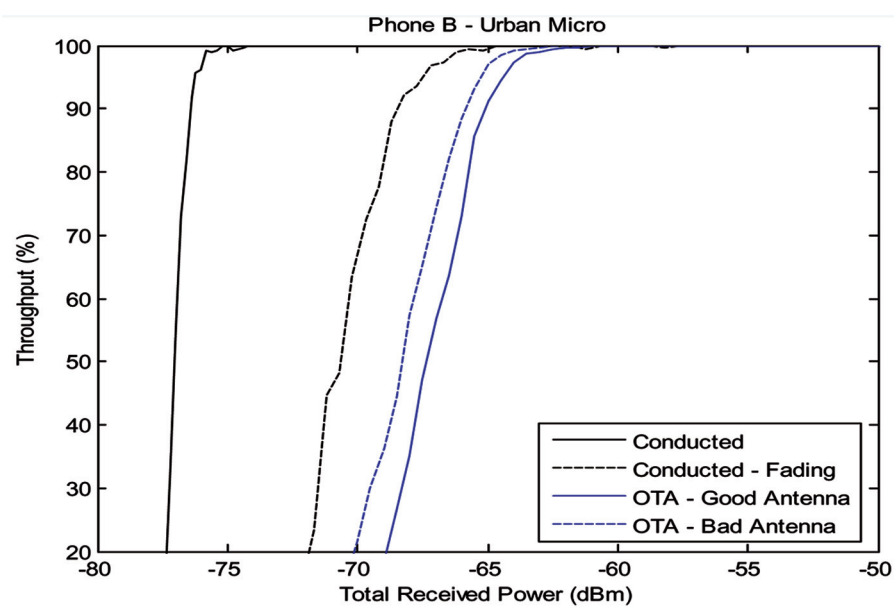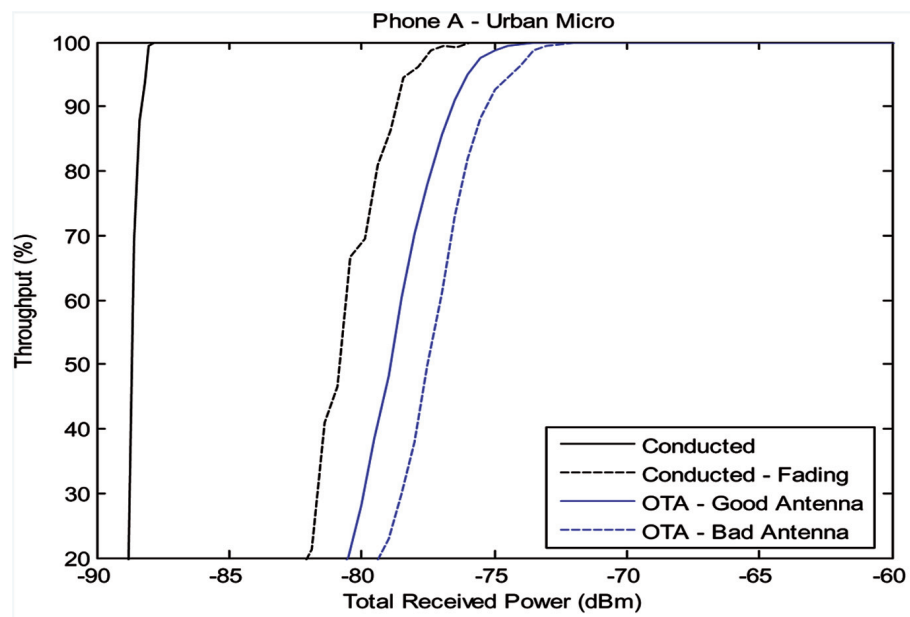
To describe the variability in the power gain patterns of a set of antennas, such as tag-like planar dipoles, a statistical model is a suitable way, which can present data in a simplified model that could be easily included in standards and in radio channel simulators. The statistical modelling of a UWB tag antenna describing the variability of its frequency averaged radiation patterns was described in Mhanna and Sibille [MS11]. The modelling is based on Fourier

series expansion in the angular domain. In the first stage, the model achieves a compression rate of more than 81 on a per antenna basis, while having a relative error smaller than 1%. In a second step, the statistical properties of the model coefficients have been extracted, allowing to further reduce the amount of parameters. Finally, the statistical model coefficients were further modelled, resulting in a final number of 32 parameters to describe the whole set of tag antenna radiation patterns.

10.5.2 Characterisation in Realistic Conditions

To achieve the full benefit that MIMO technology has promised theoretically, besides good antenna designs, a series of conditions need to be satisfied in both the propagation environment and the devices [VMS09]. A joint evaluation of MIMO antennas with the actual device and the working environment has been performed in Sánchez-Heredia et al. [SPTG13]. Two MIMO antennas, labelled as 'good' and 'bad' according to their MIMO properties and radiation characteristics in the chamber, were used for comparison. The evaluated was performed for two phones [a recently released phone A (good phone) and a first generation LTE phone B (bad phone)] whose antennas were replaced by the good or bad MIMO antennas as well as two scenarios, i.e., Urban Micro and Urban Macro. The throughput of the system is shown in Figure 10.12. For phone A, good antenna shows a consistent improvement of about 2 dB for both scenarios over the bad antenna. For phone B, the good and the bad antenna give almost the same throughput performance for the Urban Macro-cell model, whereas for the Urban Micro-cell model, the bad antenna even performs slightly better than the good one. Thus, a bad LTE device can actually mask the benefits that a good antenna design provides, or even making a bad antenna look better than a good design.

Due to the importance of the scenarios, channel characterisation is of high interest for MIMO systems. For short range communications [LN10], near field channel characterisation is necessary since the classical assumptions of IID Rayleigh do not apply anymore. A channel for a 2×2 MIMO system in near field communication is measured in Gvozdenovic et al. [GTB12]. Three antenna sets including bicone antennas, monopole and loop pair, and dipole and slot pair are utilised to obtain the channel matrix, with which channel capacity and eigenvalues of the channels were calculated. The main results are summarised in Table 10.1. The dipole/slot antenna set behaves best out of three pairs, i.e, low-pattern correlation results in increase of spectral efficiency.
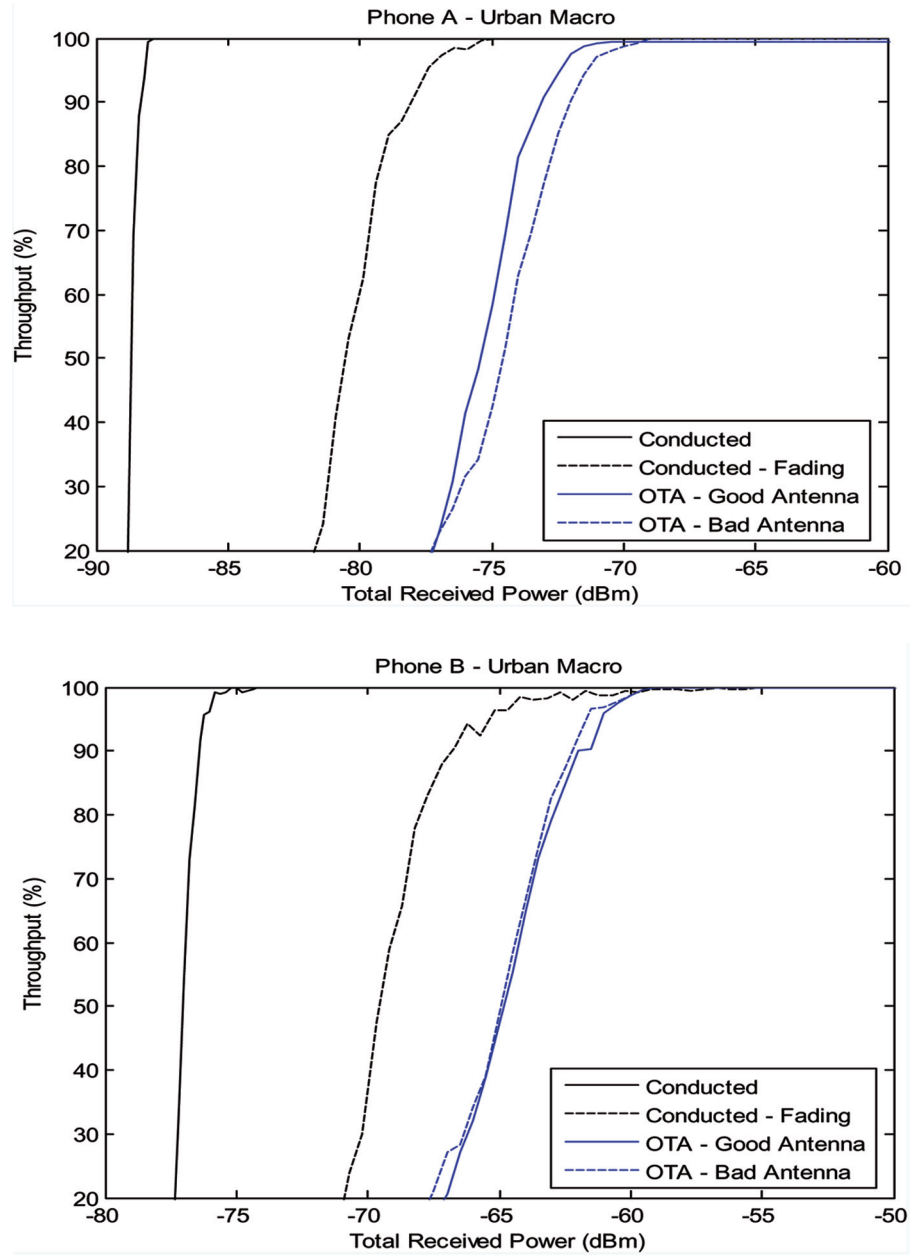
Phone A - Urban Micro

Phone B - Urban Micro

Figure 10.12 Measured LTE through put for different phones and different environments.

Table 10.1   Channel for different antenna sets

Antenna Set	ρ	d(m)	η(bit/s/Hz)	$\lambda_2 - \lambda_1$ (dB)
Bicone co-pol	1	0.7	6	15
Mono/loop 1	0.97	0.7	4	23
Dipole/slot 1	0.1	0.7	8	5

For wideband communication systems, group delay variation versus frequency is an essential issue which can cause distortion and degradation in the signals [Kwo06]. Recently, it was raised in Bahramzy and Pedersen [BP13] that group delay can also become a concern for high-Q antennas, due to its big and steep phase change over frequency. The results showed that the group delay of a low-Q antenna (dipole antennas) is around 1.3 ns, whereas a high-Q antenna (patch antenna) has group delay of around 22 ns. Therefore, it is important to measure the group delay for high-Q antennas in order make sure that its variations are within the specifications of the radio system design.

Interaction with nearby object and device mobility can also change the antenna performance as well as other components on the devices, such as EB duplexer, which can provide high Tx–Rx isolation over wide bandwidths [AGL13]. The variation in antenna impedance changes the performance of the duplexer, in terms of bandwidth and achievable isolation. When in proximity of the users, there is variation of up to 25 dB in mean isolation across a 20 MHz bandwidth [LB14], as indicated by the circuit simulations incorporating measured antenna S11 data. Interestingly, objects in the near field, especially user interaction, can improve the isolation of the duplexer. This is due to the reduction in radiated power from the antenna, which reduces the reflections from objects at further distances. Significant variation of mean Tx–Rx isolation was also observed when the device is moving, with higher device speeds causing more rapid variations [LHB$^+$14]. The performance variation also depends on the operational environment and the dynamic balancing network. The environment with higher reflection (e.g., lab) causes significantly more variation in Tx–Rx isolation than the environment with lower reflection (e.g., cafe), as shown by Figure 10.13. When the balancing network is not dynamically updated, duplexer performance is reduced by up to 12 dB compared to an ideally balanced duplexer.

Regarding real integrated mobile devices, radio performance of popular smart-phones as well as the more classical phones has been investigated with head and hand phantoms [TP13, PT14]. Total isotropic sensitivity (TIS) is used as the criteria to compare the phones. It has been observed that the
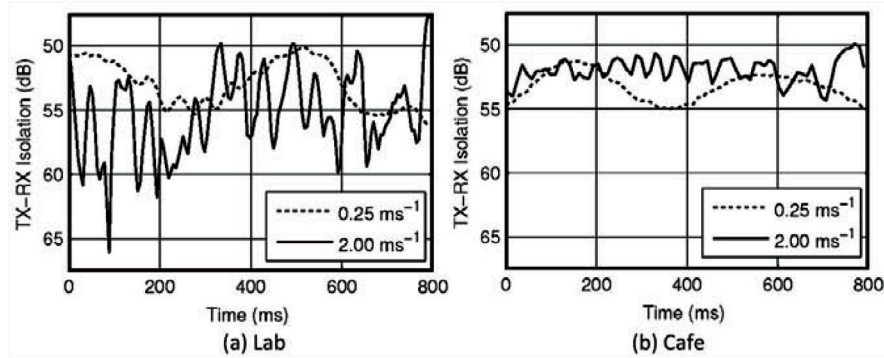
Figure 10.13 Simulated mean Tx–Rx isolation in two different environments and at two different device speeds.

newer generation thin smartphones perform worse than the classical phones, and there is even a loss in performance between generation of the same brand of smartphones. For example, the latest generation of the Galaxy and iPhone suffers 5 dB loss with respect to the last generation, which means that a doubling of the mobile base stations is required to provide the same coverage. Comparing different brands of phones, the Sony phones have very good performance among the ones used for this study, whereas the iPhones and most of the Samsung phones dominate the bottom of the performance list. Generally, the spread of TIS for most phones in all bands is within 6 dB, and half of them is within 4 dB.

10.5.3 User Effect on Antenna Systems

User effect is an important topic for terminal antennas, as it changes the antenna performance dramatically, or the user even becomes part of the antenna. The user's hand and head can lead to impedance mismatch and also greatly reduce the radiation efficiency of the antenna through absorption, deteriorating the communication performance. Figuring out how the antenna is affected by the users can provide useful information for the adaptive impedance matching of the antenna system.

The absorption loss and the mismatch level depend on the antenna type, user hand and head size and the grip style. Pelosi et al. [PFP12] compares the user effect on high-Q and low-Q antennas. The reference antenna is a PIFA, with its Q factor modified by reducing the height of the PIFA

(high-Q antenna) and adding a capacitor between the PIFA and the ground plane (tunable high-Q antenna). Both data mode and talk mode were investigated, with two-hand grips, i.e., holding the phone tight or loose. It was observed that high-Q antennas only detuned slightly for both hand grips, so that the mismatch loss is below 1 dB. Nevertheless, the total losses are not improved because the absorption losses in the high-Q antennas are higher than in the low-Q antenna. The tunable high-Q antenna has a similar behaviour, i.e., the detuning is reduced by 95%, yet the absorption loss is larger. This indicates that the three antenna models have quasi-equal total losses for all simulation environments.

The influence of the index finger's position on different antenna sets have been studied in Buskgaard et al. [BTB$^+$14b]. Simulation are carried out for both single antenna and MIMO antennas in the talking mode. For the single antenna study, antennas with different bandwidth (NB or wide band (WB)) are either top mounted (TM) or bottom mounted (BM) on the mobile handset. As shown by Figure 10.14, the total loss is about 18 dB for TM and 11 dB for BM antennas and slightly worse for WB than for NB antennas. For the MIMO antenna cases, one main antenna is placed either at the top or at the bottom, and a diversity antennas is on the side of the mobile phone. It turns out that the diversity antenna is detuned significantly, whereas the main antenna is less affected by the user though it still suffers up to 6.4 dB of mismatch loss.

In real life, the natural grip position is quite related to the size of the mobile phone. For a slim mobile phone, the index finger normally has a limited reach,
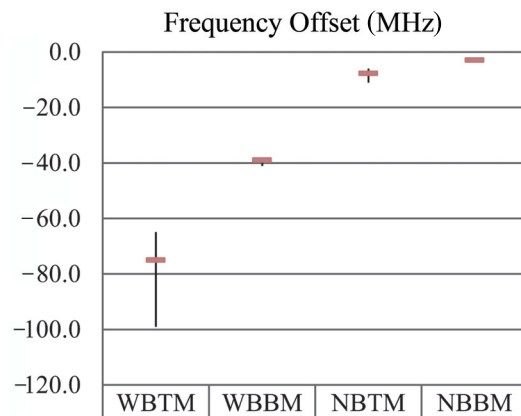

Figure 10.14   Total loss of the four antenna configurations.

i.e., it is actually shifted down from the top antenna. In this case, the factors that make NB and WB antennas perform differently with users were studied in Buskgaard et al. [BTB⁺14a]. Those factors includes power absorbed in the hand, head, plastic cover, index finger and the finger tip. As the mobile phone industry progresses, the mobile phones become larger and thinner [RE12]. For wider mobile phones, the index finger can again touch the end of phone, as in the case of Buskgaard et al. [BTB⁺14b].

Besides the antenna itself, the decoupling network connected to antennas also interact with the users, which was considered in Tatomirescu et al. [TPFP12]. When the antennas with a lumped decoupling network is in the proximity of the user, the performance of the decoupling network is degraded considerably due to the limited bandwidth of the antenna system. To counteract this degradation, either a tunable decoupling network must be implemented or the antenna placement and distance from the user must be optimised. It is also found that a distributed decoupling network is more robust than a lumped one against the user presence. Nevertheless, if the antenna position is not optimised considering the user, the decoupling network performance is still affected considerably.
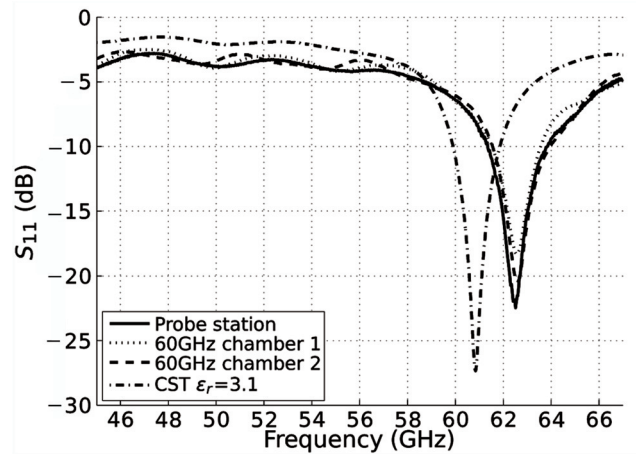
Aside from the antenna performance, the exposure of the body to a RF electromagnetic field is also important for the sake of safety. To evaluate the exposure, the metric of specific absorption rate (SAR) is used, which is defined as the power absorbed per mass of tissue. The SAR performance of MIMO-enabled mobile handsets for the body-worn case was evaluated and compared for different antenna locations and types in Li et al. [LTDL14]. The results showed that stand-alone SAR and average simultaneous SAR give the same trend for SAR values. For antenna location, different from the intuition, the co-located and separated antenna setups have similar SAR values. For antenna type, the PIFA gives a lower SAR value in general than the monopole antenna. However, the smaller bandwidth of PIFA also needs to be taken into account since it may be severely detuned when it is placed close to the body. In practice, it is challenging to measure the simultaneous SAR when multi-antennas are transmitting due to the need to account for power allocation and relative phase among the antennas. A new metric time averaged simultaneous peak SAR (TASPS) is defined in Li and Lau [LL15] to circumvent simultaneous SAR evaluation, taking advantage of the random and fast-varying channel-dependent MIMO precoding. It is shown that TASPS will satisfy the SAR limit by default, as long as the stand-alone SAR of every individual antenna satisfies the limit. Hence, only stand-alone SAR measurement is needed.

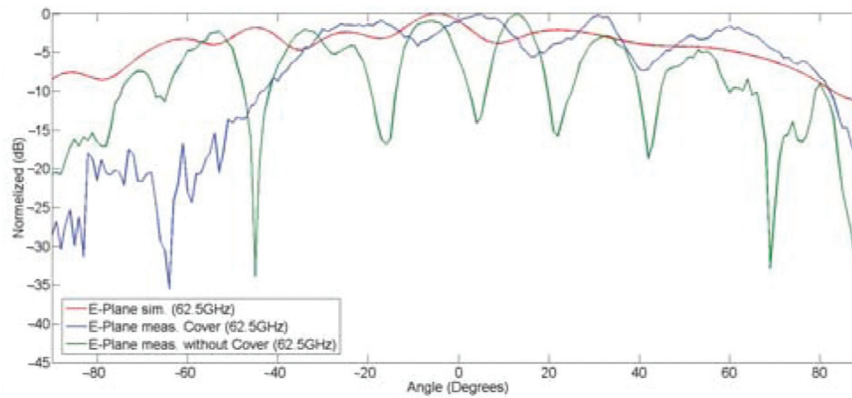## 10.6 Antenna Measurement Techniques

10.6.1 Measurement Hardware-Induced Pattern Distortions

The art of antenna measurements evolves with emerging antenna technologies, frequencies and mathematical methods. One trend in communications is the shift to higher frequencies which demands low- and medium-gain antennas at mmW frequencies. An example is the patch antenna presented in [HHS12] designed for the 60 GHz WLAN band, manufactured on a liquid crystal polymer (LCP) substrate. To rule out permittivity uncertainties as a cause of discrepancies between simulation and measurement results, the substrate panel carrying the antennas was additionally covered with 35 microstrip ring resonators. Using the measured dimensions of the manufactured resonators, the average permittivity of the panel was found to be $\varepsilon_r = 3.102$ with a standard deviation of $\sigma = 0.0143$. This permittivity is then used to simulate the antenna again, which still shows a discrepancy as indicated in Figure 10.15(a). In fact, the discrepancy is caused by manufacturing tolerances of the lithographic process which were measured as ± 30 µm at maximum using a microscope. Further discrepancies were observed on the measured pattern, whose source was clearly identified as the probe used to connect the microstrip line on the substrate with the coaxial signal source of the measurement system (Figure 10.16(b)). This issue is further discussed in Renier et al. [RvDHH13, RvDHH14b] where the radiative, reflective and obstructive properties of the probe are examined (Figure 10.15(b)). The probe poses an additional source of radiation, which creates the interference ripple indicated in the green curve in Figure 10.15(b). Covering the probe with foam absorbers reduces the ripple (blue curve) but the obstruction for $\theta < -30°$ remains. The issue is solved by a bent probe as reported in Renier et al. [RvDHH14a]). The disturbing effects of the bent probe on the radiation pattern measurements are negligible.

Pattern discrepancies and ripple do not only occur at mmW frequencies, but also arise when low-gain antennas are measured on a θ over φ scanner with limited ($-160° < \theta < 160°$) scan range, as is reported in Lasser and Mecklenbräuker [LM14]. In this survey the 14 measurements of the same AUT at different mounting positions are evaluated. The goal is to find the required Rohacell foam spacer height between the antenna under test (AUT) and the dielectric support structure to receive consistent pattern measurements, using the measurement setup shown in Figure 10.17(a). However, the measurement series reveals that increasing the spacer length itself does not improve the ripple in the θ domain. Instead, the θ ripple is increased when the AUT

(a) Return loss of the patch antenna, compare to [HHS12].

(b) E-plane radiation pattern comparison: Simulatation vs. measurement [RvDHH13].

Figure 10.15 Return loss and pattern measurement comparison of the patch antenna manufactured on LCP substrate.

is not mounted in the scanner's coordinate system centre, due to a larger resulting maximum radial extend (MRE) and less filtering in the spherical domain. Further investigations [LLM14b] reveal the θ near-field truncation as one error source. In the near-field to far-field transform the truncation acts as a step function on the measurement data which produces a Gibb's phenomenon in the far-field data. This truncation effect is extenuated when the AUT's main lobe points towards the ceiling and the truncation occurs in areas of low radiation from the AUT. To enable different orientations without
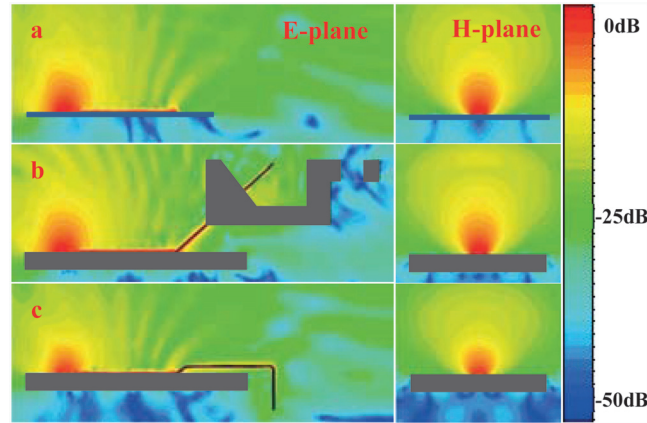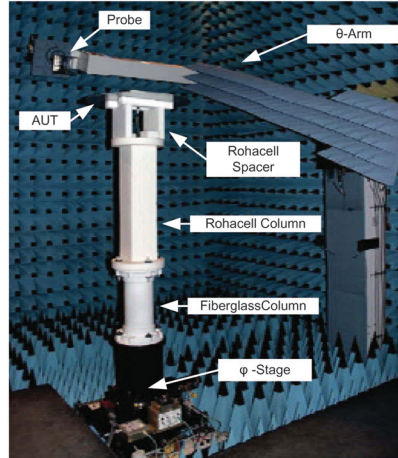
Figure 10.16   Power density comparison for: (a) ideal antenna, (b) antenna using classical probe feed, and (c) antenna fed by bent probe [RvDHH14a].
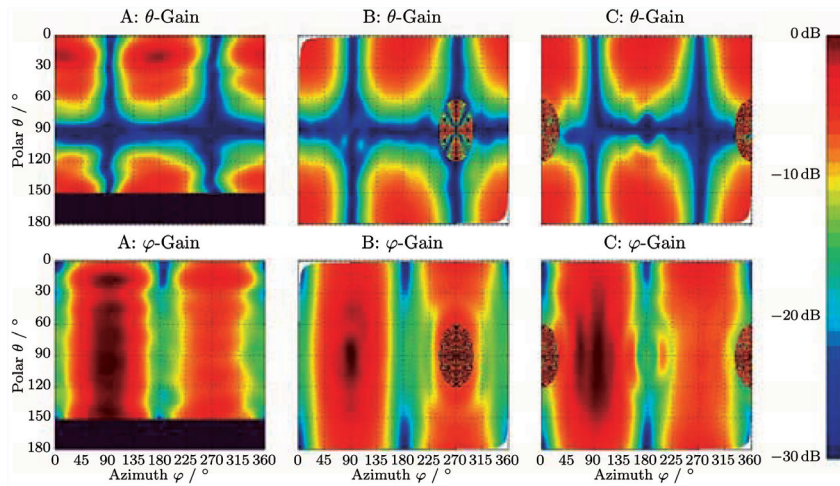
additional errors due to the feed cable, the AUT is fed using a small battery powered oscillator as described in Lasser et al. [LLM14a]. With this method the comparison shown in Figure 10.17(b) is produced, where the measurement data in orientations B and C are converted to the coordinate system A for comparison. The least ripple is produced in orientation B where the AUT's main beam points toward the ceiling of the chamber. The final solution to this measurement problem is reported in Lasser et al. [LLM15]. Using the same hardware setup (Figure 10.17(a)) and mounting the AUT offset in the z-axis, a measurement with a large MRE is obtained. The transformed far-field data is then phase shifted to mathematically move the AUT in the coordinate centre. This shifted far-field measurement data is now filtered in the spherical wave domain and again transformed into the far-field. The resulting ripple-free measurements are presented in Lasser et al. [LMPM15].

10.6.2 Efficiency Measurements for Small AUTs

Instead of using a small oscillator, a fibreoptic system as presented in Yanakiev et al. [YØCP10, YNCP12] can be used to feed an AUT without cable impairments. This is especially important to obtain accurate gain and pattern measurements for electrically small AUTs and omnidirectional radiators. The setup presented in Figure 10.18(a) is designed for a receiving AUT suitable for long range transmissions while maintaining a high SNR. The receiving AUT concept is chosen because no power hungry power amplifier is required in the small ($40 \times 40 \times 10$ mm) battery-driven unit connected to the AUT.
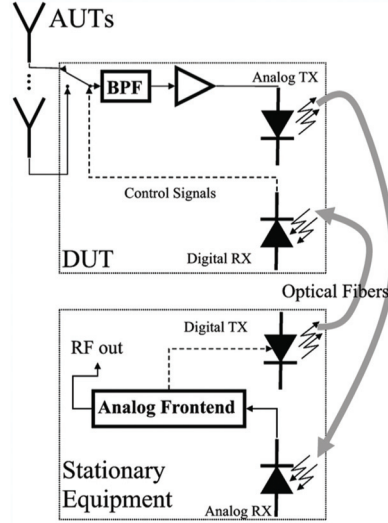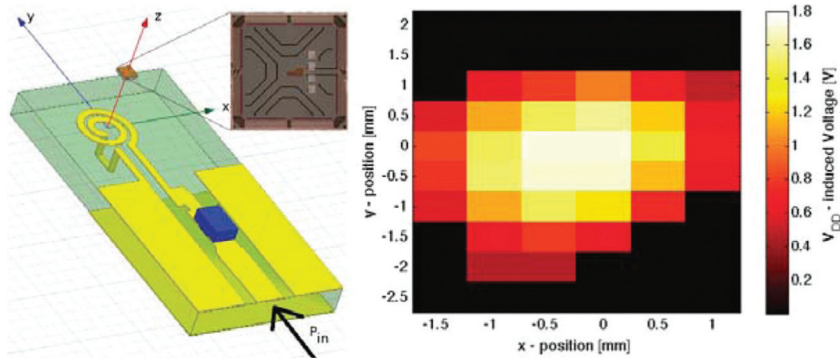
(a) Measurement setup.

(b) comparison of gain plots in three mounting configurations, tranformed
to coordinate system A.

Figure 10.17 Measurement setup and gain plot comparison of same AUT in three mounting configurations, transformed to coordinate system A [LLM14b].

This setup supports a high-power Tx on the other side of the channel, while the signal received at the AUT is amplified, directly modulates a laser diode, and is converted back to an electrical signal at the stationary equipment with an overall gain of 10.1 dB at 776 MHz. At this frequency the overall dynamic range of the presented optical feed system is 39 dB.

(a) Block diagram for the long range receiving AUT configuration [YØCP10].

(b) Contactless evaluation of the induced voltage of a tiny RFID tag with on-chip antennna [GHSM12b].

Figure 10.18   Two different approaches for measuring AUT efficiencies.

While the presented optical solution is very compact and, therefore, supports many ESAs, extremely small AUTs such as on-chip devices still cannot be characterised with such a solution. A different approach is presented in [GHSM12b, GHSM12a]: For the development of a single chip RFID tag with an on-chip antenna measuring $1 \times 1\text{mm}^2$, a contactless evaluation method is required to analyse the on-chip antenna and the rectifier for the setup's

efficiency. The circuitry of the developed evaluation platform is designed so that the modulation frequency of the signal backscattered from the chip is proportional to the induced voltage V_{DD} of the rectifier which is delivered from the on-chip antenna. For the actual measurement the chip is moved in the $x-y$ plane at a constant height above the excitation coil (see left side of Figure 10.18(b)). At each point of the measurement grid, the modulation frequency is measured and subsequently V_{DD} is calculated. The result can be seen in the right side of Figure 10.18(b), where the chip was in a height $z = 0.5$ mm above the excitation coil. In this $x-y$ plane a maximum induced voltage of 1.7 V is measured, where the input power at the excitation coil is $P_{in} = 8.6$ dBm.

Besides this method to measure the performance of an on-chip antenna and the connected the rectifier based on voltage mapping, a more conventional approach is to enclose the AUT in a cavity – called Wheeler cap – and measure the altered return loss at the antenna port. Comparing this value to the free space return loss, the efficiency of the AUT is obtained. However, for fixed cavity geometries, the bandwidth of the Wheeler method is limited, due to cavity resonances of the Wheeler caps. In Kakoyiannis and Constantinou [KC12a], an extensive survey on the achievable bandwidth of this method is presented, given the dimensions of the AUT. For rectangular cavities operated below cut-off, flat AUTs with dimensions of 0.6 $\lambda_0 \times 0.3 \lambda_0$ are measurable. Using the intermodal spectrum, the AUT geometry may reach 0.78 $\lambda_0 \times 0.39 \lambda_0$, achieving 33% of measurement bandwidth. Using spherical Wheeler caps, bandwidths up to 84% are obtained for small AUTs.